



Updated SO₂ emission estimates over China using OMI/Aura observations

Maria Elissavet Koukoul¹, Nicolas Theys², Jieying Ding^{3,4}, Irene Zyrichidou¹, Bas Mijling³, Dimitrios Balis¹ and Ronald Johannes van der A³

¹Laboratory of Atmospheric Physics, Aristotle University of Thessaloniki, Greece.

²Royal Belgian Institute for Space Aeronomy (BIRA-IASB), Brussels, Belgium.

³Royal Netherlands Meteorological Institute (KNMI), De Bilt, The Netherlands.

⁴Technical University Delft, Delft, The Netherlands

Abstract

The main aim of this paper is to update existing sulphur dioxide (SO₂), emission inventories over China using novel inversion techniques, state-of-the-art chemistry transport modelling (CTM), and satellite observations of SO₂. Within the framework of the EU FP7 *Monitoring and Assessment of Regional air quality in China using space Observations*, MarcoPolo project, a new SO₂ emission inventory over China was calculated using the CHIMERE v2013b CTM simulations, ten years of OMI/Aura total SO₂ columns and the pre-existing Multi-resolution Emission Inventory for China (MEIC v1.2). It is shown that including satellite observations in the calculations increases the current bottom-up MEIC inventory emissions for the entire domain studied [102° to 132°E and 15° to 55°N] from 26.30 Tg/annum to 32.60 Tg/annum, with positive updates which are stronger in winter [~36% increase]. New source areas were identified in the South West [25-35°N and 100-110°E] as well as in the North East [40-50°N and 120-130°E] of the domain studied as high SO₂ levels were observed by OMI, resulting in increased emissions in the a posteriori inventory that do not appear in the original MEIC v1.2 dataset. Comparisons with the independent Emissions Database for Global Atmospheric Research, EDGAR v4.3.1, show a satisfying agreement since the EDGAR 2010 bottom-up database provides 33.30 Tg/annum of SO₂ emissions. When studying the entire OMI/Aura time period [2005 to 2015 inclusive], it was shown that the SO₂ emissions remain nearly constant before year 2010 with a drift of -0.51±0.38 Tg/annum and show a statistically significant decline after year 2010 of -1.64±0.37Tg/Annum for the entire domain. Similar findings were obtained when focusing on the Greater Beijing Area [110° to 120°E and 30° to 40°N] with pre-2010 drifts of -0.17±0.14 and post-2010 drifts of -0.47±0.12Tg/annum. The new SO₂ emission inventory is publicly available and forms part of the official EU MarcoPolo emission inventory over China which also includes updated NO_x, VOCs and PM emissions.



1 Introduction

2

3 Due to its undoubtable rapid economic growth, swift urbanization and consequent enlarged energy
4 needs, large parts of China have been suffering from severe and persistent environmental issues
5 including major air pollution episodes (Song, et al., 2017.) Developing and implementing effective air
6 quality control policies is essential in combating such pollution problems and requires timely as well as
7 dependable information on emission levels (Zhang et al., 2012; van der A, et al., 2016.) Understanding
8 and monitoring the local long-term trends of different atmospheric pollutants is paramount in
9 updating, and predicting, pollution emission scenarios (Kan, et al., 2012.) Satellite atmospheric
10 observations have recently become an important information source for the atmospheric state, not
11 only of the academic community, but also by public authorities and international environmental
12 agencies (Streets et al., 2013; Lu and Liao, 2016). Recent reductions of the two major pollutants emitted
13 mainly by industrial sources, nitrogen and sulphur dioxide, have already successfully been observed
14 and quantified in a usable manner from space-born instruments over China (Wang et al., 2010; 2015,
15 Liu et al., 2015; 2017).

16 Sulfur dioxide, SO₂, is released into the atmosphere through both natural and anthropogenic
17 processes. In the former category lie chemical processes, such as the reaction of hydrogen sulfide with
18 the atmospheric oxygen, seasonal biomass burning events, which may be foreseen to some extent, if
19 not modelled, as well as volcanic degassing and unexpected eruptions (see for e.g. Seinfeld and Pandis,
20 1998). In the latter category fall the combustion of coal and oil fuel which account for more than 75%
21 of global SO₂ emissions (Klimont et al., 2013), a figure found to be similar when focusing on the Chinese
22 domain (Smith et al., 2001; 2011). Lu et al., 2011, showed that SO₂ emissions over China, calculated from
23 all major anthropogenic sources as well as scheduled biomass burning events, increased from ~24 Tg
24 in year 1996 to ~31 Tg for year 2010, including fluctuations due to the onset of environmental
25 protection measures as well as the international economic crisis. The balance between encouraging
26 China's economic development and dealing with its environmental side-effects often causes irregular
27 changes in the SO₂ emitted amounts, further dependent on the Province observed.

28 Satellite SO₂ observations have proven to be a reliable way to monitor emissions from space and are
29 increasingly used in order to update bottom-up emission inventories (Streets et al., 2013). Numerous
30 works have already amply demonstrated the ability of satellite sensors to observe regional
31 anthropogenic emission sources such as studying the SO₂ load over China using OMI/Aura
32 observations (Krotkov et al., 2008; Witte et al., 2009; Li et al., 2010; Jiang et al., 2012; Fioletov et al.,
33 2013; 2016.) Following their lead, in this work we aim to present a new spatially-resolved SO₂ emission
34 inventory on a monthly time scale for years 2005 to 2015 based on satellite observations and modern
35 chemical transport modelling simulations.

2 Data Description

37

38 The mathematical analysis used in this work in order to extract updated SO₂ emission fields is fully
39 described in Section 3. The main gist is that three inputs pieces of information are required; an original,



1 also known as *a priori*, emission inventory, the satellite observations of the SO₂ load and SO₂ profiles
2 provided by an air quality chemistry transport model. The quality of these three pieces of information
3 ensures the accuracy of the updated, *aposteriori*, SO₂ emissions estimates. Since the mathematical
4 formulism requires also quantifiable error estimates on these three input parameters, using the new
5 OMI/Aura BIRA SO₂ dataset [Theys et al., 2015; 2017] ensures that the satellite observations used here
6 are fully characterized in this manner. In Sections 2.1 to 2.3 the three input datasets are presented and
7 discussed appropriately.

8 **2.1 The MEIC emission inventory**

9

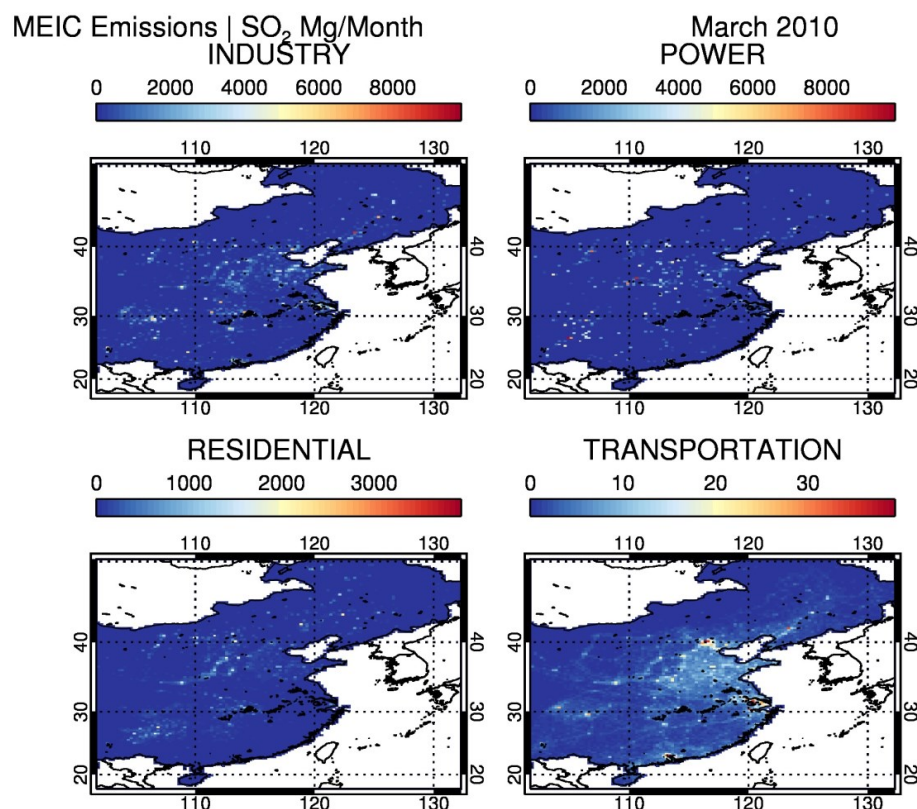
10 The Multi-resolution Emission Inventory for China (MEIC v1.2) model has been developed for years
11 2008, 2010 and 2012, by the School of Environment, Tsinghua University, Beijing, China and is
12 downloadable from <http://www.meicmodel.org/>. SO₂ emissions, in Mg/month, are calculated on a
13 monthly basis for four sectors: power, industry, residential, and transportation, in a spatial resolution
14 of 0.25x0.25 degrees. The domain applicable spans from 102°E to 132°E and from 15°N to 55°N. For the
15 requirements of the methodology applied here the error on these emissions has been assumed to rise
16 to 50% of the actual reported value.

17 An example of the SO₂ MEIC v1.2 emissions in Mg/month for March 2010 is shown in Figure 1. The
18 relative strength of the four sectors is shown as well, with industry on the top left panel, the power
19 sector on the top right, the residential emissions in the bottom left and transportation in the bottom
20 right. Different colour scales in the panels were used for the different emission strengths. In Zhang et
21 al., 2015, the 2010 MEIC v1.2 emissions have been used as spin-up information in order to perform
22 sensitivity simulations with different SO₂ emission reduction scenarios. It was shown that reducing SO₂
23 emissions from one region has a small effect on SO₂ concentrations over the other regions. The
24 national mean SO₂ concentration however is most sensitive to SO₂ emissions from Northern China, in
25 this work called the Greater Beijing Area. This strengthens the importance of providing accurate and
26 updated emission levels over that region in China even though it is considered to be the best
27 represented within existing inventories.

28

29

30



1

2 Figure 1. The SO₂ MEIC v1.2 emissions in Mg/month for March 2010. The relative strength of the four
3 sectors is shown here; industry, top left; power, top right; residential, bottom left and transportation,
4 bottom right. Note the different colour bars used.

5

6 2.2 The OMI/Aura SO₂ observations

7

8 The Ozone Monitoring Instrument (OMI) is a nadir-viewing instrument on board the NASA Aura
9 satellite flying in a Sun-synchronous polar orbit with an equator crossing time of around 13:30 local
10 time in the ascending node launched in July 2004. The OMI imaging spectrograph measures
11 backscattered sunlight in the ultraviolet-visible range from 270 nm to 500 nm with a spectral resolution
12 of about 0.5 nm [Levelt et al., 2006]. The OMI spatial swath is around 2600 km wide achieving near-
13 complete global coverage in approximately one day. The OMI ground pixel size varies from 13 × 24 km²
14 at nadir to 28 × 150 km² at the edges of the swath. Since June 2007, the radiance data of OMI for some
15 particular viewing directions have been corrupt, a feature known as the *OMI row anomaly*



1 (<http://www.knmi.nl/omi/research/product/rowanomaly-background.php>). Hence, the suggested
 2 OMI observations are excluded de facto from the analysis.

3 In this work, we employ the retrieved SO₂ Vertical Column Densities (VCDs) using the Royal Belgian
 4 Institute for Space Aeronomy, BIRA, algorithm [Theys et al., 2015] which are calculated using the
 5 Differential Optical Absorption Spectroscopy (DOAS) technique [Platt and Stutz, 2008] to the
 6 measured spectra in the 312–326 nm wavelength range. This step is followed by data filtering for the
 7 row anomaly issue and a background correction to account for possible biases on the retrieved slant
 8 columns. The obtained quantity is converted into a SO₂ VCD using an air mass factor, AMF, which
 9 accounts for changes in measurement sensitivity due to observation geometry, ozone column, clouds,
 10 and surface reflectivity. The anthropogenic SO₂ profile required in the AMF calculation has been
 11 extracted from the IMAGES tropospheric chemistry transport model [see Stavrakou et al., 2013, and
 12 references therein]. All details on the BIRA OMI SO₂ algorithm can be found in Theys et al. [2015]
 13 updated recently in Theys et al., 2017. The dataset has already been employed in different studies; in
 14 van der A et al. [2016] in order to estimate the effectiveness of current air quality policies for SO₂ and
 15 NO_x emissions in China; in Koukouli et al., 2016, in order to quantify the anthropogenic SO₂ load over
 16 China using different satellite instruments and algorithms; in Schmidt et al., 2015, in order to study the
 17 2014–2015 Bárðarbunga-Veiðivötn fissure eruption in Iceland, among others.

18 The domain considered extends from 102° to 132°E and from 18° to 50°N and covers Eastern China. Daily
 19 observations were filtered for high Solar Zenith Angle, SZA, of > 70°, cloud fraction of > 0.2 and also
 20 SO₂ algorithm flagging, as per Theys et al. [2015]. The filtered data were then averaged onto a
 21 0.25°x0.25° monthly grid using a 0.75° smoothing average box. For further details on this pre-
 22 processing refer to Koukouli et al. [2016].

23 Within the OMI BIRA SO₂ product, error contributions resulting from each step of the retrieval to the
 24 final vertical column error are provided separately, including their random and systematic parts [Theys
 25 et al., 2017]. This allows the estimation of the total error on the column averages, an important feature
 26 in this analysis where the instantaneous OMI observations are gridded and then averaged on a
 27 monthly mean basis. The formulation of the error on the vertical SO₂ column is derived by basic error
 28 propagation, shown in Eq. (1).

$$\sigma_{N_V}^2 = \left(\frac{\sigma_{N_S}}{M}\right)^2 + \left(\frac{\sigma_{N_S^{\text{back}}}}{M}\right)^2 + \left(\frac{(N_S - N_S^{\text{back}})\sigma_M}{M^2}\right)^2 \quad (1)$$

29

30 where σ_{N_S} , σ_M and $\sigma_{N_S^{\text{back}}}$ are the errors on the slant column, N_S , the air mass factor, M , and N_S^{back} the
 31 reference correction, respectively. When averaging the observations, the systematic and random
 32 components of each given error source need to be discriminated and so Eq. (1) evolves into Eq. (2)

33

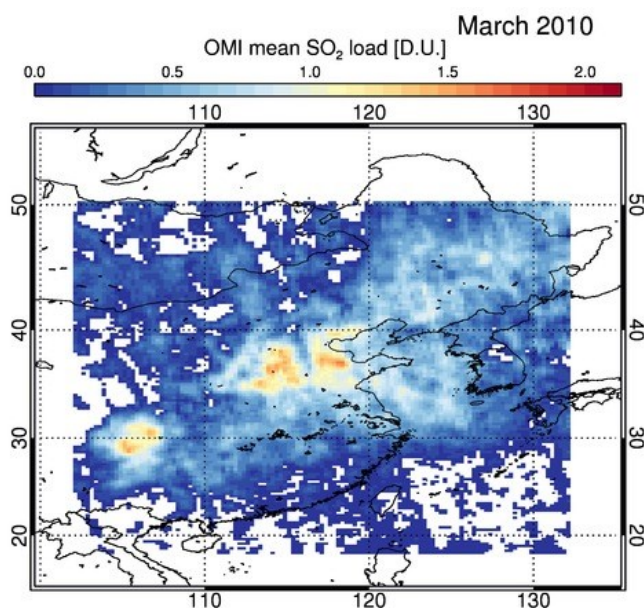
$$\sigma_{N_V}^2 = \frac{1}{M^2} \left(\sigma_{N_S\text{-syst}}^2 + \frac{\sigma_{N_S\text{-rand}}^2}{N} + \frac{\Delta N_S^2}{M^2} \sigma_{M\text{-syst}}^2 + \frac{\Delta N_S^2}{M^2} \frac{\sigma_{M\text{-rand}}^2}{N} \right) \quad (2)$$

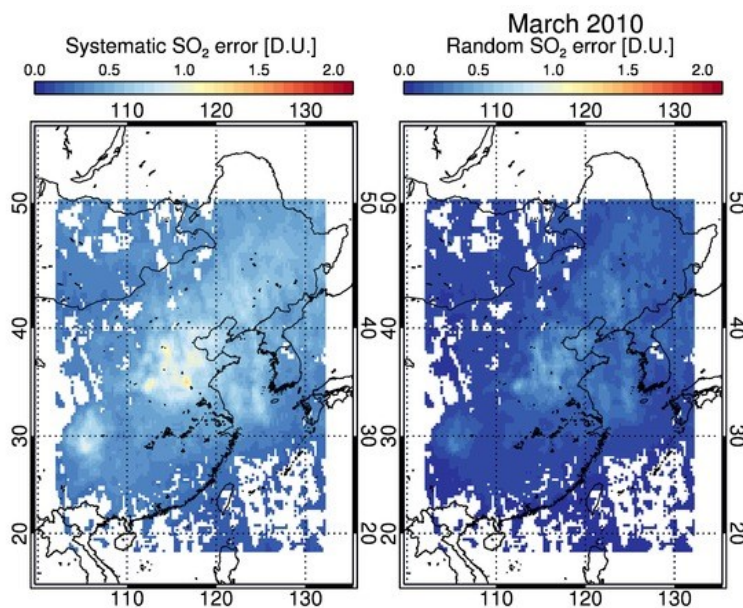
34



1 where N is the number of ground pixels considered in the average and $\sigma_{N_{S_syst}}$ is the systematic
2 uncertainty on the slant column density, SCD, which also includes the systematic uncertainty
3 associated to the background correction. The Vertical Column Density, VCD, is denoted by N_v ; the SCD
4 by N_s ; the SCD correction by $N_{s,0}$; the SCD-SCD correction by ΔN_s ; the AMF by M ; the VCD precision
5 by σ_{NV} ; the SCD precision by σ_{NS_rand} ; the AMD precision by σ_{M_rand} and the AMF trueness by σ_{M_syst} . The
6 error analysis is accompanied by the total column averaging kernel (AK) calculated as the weighting
7 function divided by the air mass factor, M [Eskes and Boersma, 2003]. The weighting function
8 characterizes the sensitivity of the extracted atmospheric column to changes in the true profile and
9 its importance in the analysis of satellite observations, alongside their correct comparison to other
10 datasets, has long been established [see for e.g. Rodgers 2000, Ceccherini and Ridolfi, 2010, Zhang et
11 al., 2010, etc.] In Section 2.3 the importance of the AKs in co-analyzing satellite observations and
12 modelling results in this work is discussed extensively.

13 An example of the OMI SO₂ product used in this work is shown in Figure 2, for the month of March
14 2010. The retrieved SO₂ VCD in Dobson Units (D.U.) is shown in the upper panel with the systematic
15 component to the error in the bottom left and the random component in the bottom right.





1 Figure 2. Upper panel: the monthly mean OMI/BIRA SO₂ columns in D.U. for March 2010. Lower panel: the
2 associated systematic error [left] and random error [right] in D.U. calculated using Eq. (2).

3 In the original work of Martin et al., 2006, which was based on GOME/ERS-2 observations and GEOS-
4 CHEM model data on a resolution of 2° by 2.5°, the authors conclude that the major limitations in their
5 work were the coarse horizontal resolution of GOME – which is not the case here for OMI– and the
6 lack of direct validation of the GOME tropospheric NO₂ product – again, not this case here as the OMI
7 BIRA SO₂ measurements have been already been verified against other satellite observations [Bauduin
8 et al., 2016; Koukouli et al., 2016] as well as long term ground-based measurements in polluted
9 locations [Theys et al., 2015, Wang et al., 2017].

10

11 **2.3 The CHIMERE model output**

12

13 A multi-scale model for air quality forecasting and simulation, CHIMERE,
14 <http://www.lmd.polytechnique.fr/chimere/>, is providing SO₂ profiles over the Chinese domain between
15 102°E - 132°E and 18°N - 50°N for the mean overpass hour of OMI/Aura over the domain. The model
16 version is CHIMERE v2013b [Menut et al. 2013] at a spatial resolution of 0.25°x0.25° and on eight vertical
17 layers in ppb, i.e. seven vertical levels, spanning from the surface up to 500hPa, for year 2010. The
18 meteorological input was provided by ECMWF, <http://www.ecmwf.int/>, operational data. The
19 anthropogenic emission inventory in this CHIMERE run was a mix of the MEIC v1.2 inventory for
20 mainland China and the Intex-B emission inventory, <http://mic.greenresource.cn/intex-b2006> for areas
21 outside China. The biogenic emissions are provided by the MEGAN database,
22 <http://lar.wsu.edu/megan/>. For the background of the particular CHIMERE set-up refer to Mijling and



1 van der A, (2012), whereas more specific details on the CHIMERE v2013b run used here may be found
 2 in Ding et al., (2015).

3 The uncertainty of the CHIMERE SO₂ columns is assumed to rise to 25%. Estimating mathematically
 4 modelling errors is quite challenging due to the large number of modelling processes and input
 5 parameters that have no defined error, such as for e.g. the boundary and initial conditions, the species
 6 emissions, rate constant uncertainties, even unresolved aspects of atmospheric physics and chemistry
 7 [Deguillaume et al., 2008; Boersma et al., 2016]. Typically such uncertainties are deduced from
 8 comparisons to other CTMs [Pirovano et al., 2012] and/or to independent observational datasets [Lee
 9 et al., 2009]. Even so, due to the innumerable differences in mathematically expressing atmospheric
 10 processes in the former case and between model simulations and observations in the latter case,
 11 calculating a definite value remains elusive. In Figure 3, upper, the March 2010, CHIMERE integrated
 12 SO₂ column is shown as example for the domain in question.

13 Before proceeding to the CHIMERE profiles convolution to the OMI AKs and subsequent vertical
 14 integration, we investigated whether the differences in orography heights assumed by the CHIMERE
 15 and OMI datasets in the respective algorithms may introduce artifacts in the final CHIMERE VDCs. Zhou
 16 et al., 2009, have shown that, for the case of NO₂ profiles retrieved from OMI measurements over the
 17 Po Valley and the Alps, the difference in orography between satellite pixel and CTM grid may lead to
 18 either over- or under-estimation of the NO₂ VCDs by between 10 and 25%. Theys et al., 2017, in order
 19 to utilize more realistic *a priori* SO₂ profiles, employed CTM model profiles at 1°x1° resolution and used
 20 the hypsometric equation (Eq. (3)) to scale them down to the future TROPOMI/S5P 7 km × 3.5 km spatial
 21 resolution. In this equation, a new effective pressure, P_{eff} , which differs from the model surface
 22 pressure P_{ERA} , is calculated under the assumption that the surface temperature, T_{ERA} , varies linearly
 23 with height with a lapse rate of $\Gamma = -6.5\text{Kkm}^{-1}$, gas constant of $R=287\text{Jkg}^{-1}\text{K}^{-1}$ and gravitational
 24 acceleration of $g = 9.8\text{ms}^{-2}$. This variation depends on the difference between the orography height of
 25 CHIMERE, h_{CHIM} , and the OMI-reported height per observation, h_{eff} . The surface pressure and
 26 temperature have been extracted from the ERA-interim dataset,
 27 <https://www.ecmwf.int/en/research/climate-reanalysis/era-interim>, on a daily temporal and 0.75°x0.75°
 28 spatial resolution [Dee et al., 2011].

29 In the case of SO₂ anthropogenic emissions, this whole issue may be significant in locations where the
 30 surface height alters significantly within our 0.25°x0.25° grid whereupon the OMI pixel may have
 31 viewed an entirely different atmospheric state, by more than ~1km in the vertical. In this work and for
 32 the entire ten years of OMI observations, only 3% of the entire domain of 15609 grid points show an
 33 over-estimation of h_{CHIM} heights above 500m and less than 0.5% of the grid points show an over-
 34 estimation of h_{eff} heights.

35

$$P_{eff} = P_{ERA} \left(\frac{T_{ERA}}{T_{ERA} + \Gamma(h_{CHIM} - h_{eff})} \right)^{-g/R\Gamma} \quad (3)$$

36

37



1 Even so, and for completeness sake, the CHIMERE profiles were re-scaled accordingly to the new
2 pressure levels, calculated from P_{eff} and the CHIMERE pressure parameters as applied in Equations 2
3 and 6 of Zhou et al., 2009. Grid points with associated CHIMERE heights of greater than 1500m, which
4 represent 7.5% of the domain, almost exclusively in the western-most part [west of 110°E] where the
5 Tibetan plateau rises, are excluded from this re-scaling due to interpolation issues. Those pixels are in
6 any case excluded in the analysis for the new emission database further on due to their non-existent
7 SO₂ contributions. Overall, the non-seasonally dependent differences found in the CHIMERE columns
8 before and after scaling were of the order to ~10-12%, on the low side of the Zhou et al., 2009, estimates
9 for NO_x who were however faced with far greater topological variabilities in the locations of their
10 study. As a consequence, we consider the convolution of modelling profiles to the satellite AK a far
11 more important factor in the solidity of the proposed methodology than anything else.

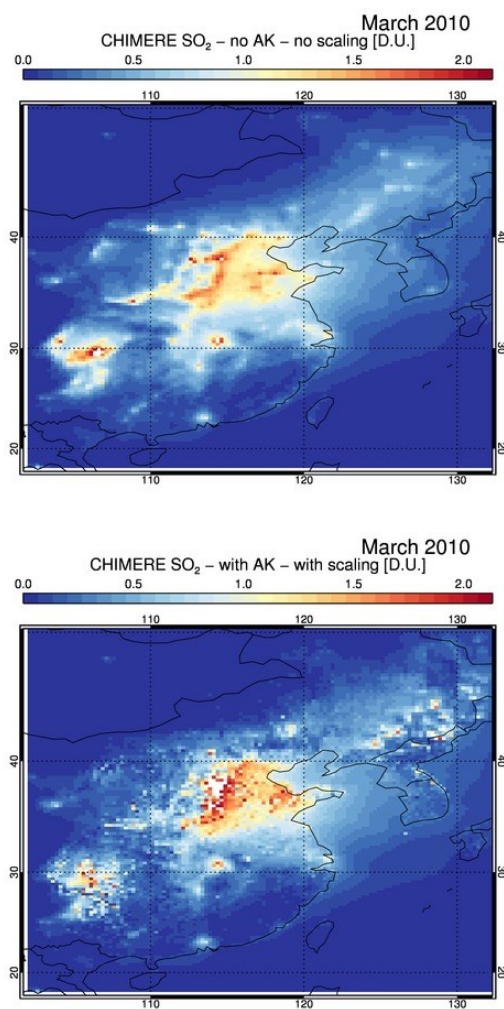
12 An extremely small fraction of our domain showed significant variation of above 0.5 D.U. in absolute
13 differences, of less than ~0.05% of the pixels for the entire domain irrespective of month, due to
14 numerical uncertainties introduced by the re-shaping, re-scaling and altering between the different
15 altitude domains of the CHIMERE and OMI profiles. Hence, for the main aim of this paper which is to
16 update SO₂ emission fields over Eastern China and not to provide absolute SO₂ emitted quantities, we
17 deem this difference well within the final emission inventory error budget discussed below in Section
18 4.1.

19 We then proceed in convolving the re-scaled CHIMERE profiles with the OMI column averaging kernel
20 as discussed in Eskes and Boersma, 2003 and Boersma et al., 2008a. The CHIMERE model profiles were
21 already in a 0.25°x0.25° monthly grid whereas the OMI observations are point daily measurements.
22 Hence, the CHIMERE profile for each grid was convolved with each of the corresponding OMI AKs that
23 fall within the same 0.25°x0.25° grid and then averaged [see Figure 3, bottom]. On average, the
24 convolution of the CHIMERE re-shaped profiles with the OMI AKs introduced a seasonally dependent
25 decrease in the SO₂ modelled levels, between ~0-5% [for the summer months] and 10-15% [for the
26 autumn-winter months] for the entire domain, as expected.

27 An example of this entire process is provided in Figure 4 for the grid box 38.0°N, 113.25°E, a location
28 slightly to the West of Greater Beijing Area with a moderate orography height of ~1km. In the left panel
29 the original CHIMERE SO₂ profile in 8 levels in ppb is shown in blue, the same profile but in Dobson
30 units per layer is given in red whereas the profile in Dobson units but on the OMI 58 AK levels is given
31 in black. The y-axis ranges up to ~5 km which is approximately the vertical range of the CHIMERE model.
32 In the middle panel the OMI AK profile is presented. In the right panel the original CHIMERE profile in
33 Dobson units is shown again in black so as to compare easily to the convolved CHIMERE profile, in olive
34 green. Insert in this panel the total SO₂ load in D.U. for the two profiles is also given. The re-shaped
35 CHIMERE total SO₂ column is 1.66 D.U. whereas after convolution with the OMI AK it decreases to 1.11
36 D.U. while the actual load is also re-structured in order to approach the atmosphere sense by the
37 satellite instrument. It is hence shown that even though the total column has not changed the vertical
38 distribution of that column does change to reflect the sensitivity of the satellite observations, which
39 peaks higher up in the boundary layer and lower troposphere.

40

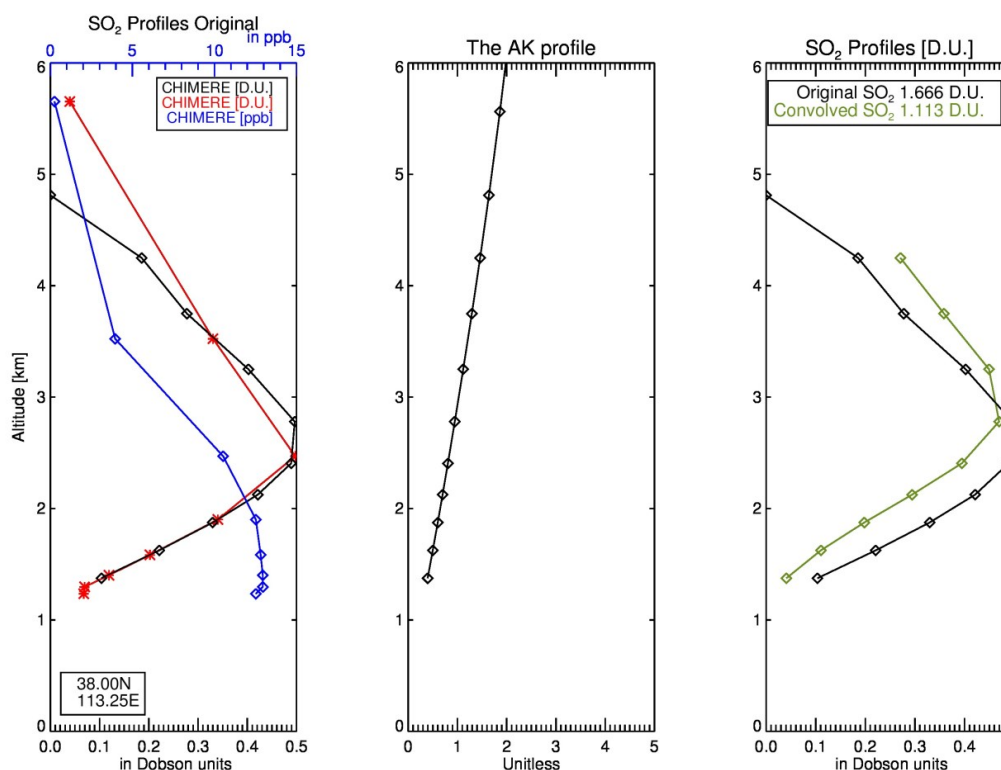
41



1 *Figure 3.* The March 2010 SO₂ columns in D.U. as integrated in height from the original CHIMERE model ppb levels:
2 upper, without rescaling to the effective pressure and without convolution with the OMI AKs; lower, with
3 rescaling and with convolution with the OMI AKs.

4

5



1 Figure 4. An example of the convolution of the CHIMERE SO₂ profile with the OMI Averaging Kernel to produce
 2 the convolved CHIMERE total SO₂ column for the grid 38.0°N, 113.25°E. Left panel: The original CHIMERE SO₂
 3 profile in 8 levels in ppb is shown in blue, the same profile but in Dobson units per layer is given in red whereas
 4 the profile in D.U. but on the OMI 58 AK levels is given in black. Middle panel: the OMI AK profile. Right panel:
 5 the original CHIMERE profile in D.U. per layer is shown in black, as in the left panel, and the convolved CHIMERE
 6 profile is D.U. per layer is shown in olive green. The original CHIMERE total SO₂ column is 1.66 D.U. whereas after
 7 convolution with the OMI AK it decreases to 1.11 D.U.

8 3 Mathematical formulism

9 3.1 Top-down and a posteriori emissions estimates

10

11 The inversion methodology applied here is the one first presented in Martin et al., 2003, and further
 12 applied in Martin et al., 2006, Boersma et al., 2008b, Lamsal et al., 2010, Lin et al., 2010, Gu et al., 2014,
 13 Zyrichidou et al., 2015, among others. The main premise of the methodology resides in the mass
 14 balance equation [Leue et al., 2001] and requires three input parameters; the *a priori* emission field, E_a
 15 [Sect. 2.1], the satellite-derived SO₂ field, Ω_t [Sect.2.2] and the model SO₂ field, Ω_a [Sect.2.3]. Using
 16 those, as per Eq. (4), the *top-down* emission inventory, E_t , is calculated. Using standard propagation



1 error analysis, the error on the *top-down* emission field may be calculated through Eq. (5), where the
 2 error on the *apriori* emissions, ε_a , is required, as well as the error on the model estimates, ε_{Ω_a} and the
 3 satellite retrieval error, ε_{Ω_t} . These error levels have been discussed in the equivalent sections.

4

$$E_t = E_a * \frac{\Omega_t}{\Omega_a} \quad (4)$$

5

$$\varepsilon_t^2 = \left(\frac{\Omega_t}{\Omega_a} * \varepsilon_a\right)^2 + \left(\frac{E_a}{\Omega_a} * \varepsilon_{\Omega_t}\right)^2 + \left(\frac{E_a \Omega_t}{\Omega_a^2} * \varepsilon_{\Omega_a}\right)^2 \quad (5)$$

6

7 The calculated *top-down* emission inventory, E_t , may be combined with the *apriori* emission inventory,
 8 E_a , to provide an *aposteriori* emission inventory, E_p , following the maximum likelihood theory and a
 9 log-normal distribution of errors. In Eq. (6) the calculation of the *aposteriori* emission inventory is given,
 10 and its associated relative error in Eq. (7). Hence, in this methodology, the original bottom-up emission
 11 inventory is combined with the top-down satellite observations, weighted by their respective errors,
 12 and using modeling outputs as background field, in order to constraint, update and provide new
 13 emissions estimates. It also follows that since the *apriori* emission field is weighted by the top-down
 14 emission field error, and vice versa, the *aposteriori* will depend mostly on the *apriori* should the errors
 15 of the top-down be too large, and vice versa. In that way, it is assured that at locations where the
 16 satellite observations are too sparse or the information content in the SO_2 load too low, the *aposteriori*
 17 emission field will revert back to the *apriori*.

18

$$\ln E_p = \frac{\ln E_a (\ln \varepsilon_t)^2 + \ln E_t (\ln \varepsilon_a)^2}{(\ln \varepsilon_t)^2 + (\ln \varepsilon_a)^2} \quad (6)$$

19

$$(\ln \varepsilon_p)^{-2} = (\ln \varepsilon_t)^{-2} + (\ln \varepsilon_a)^{-2} \quad (7)$$

20

21 We should clarify at this point that the calculations of Eq. (4) to Eq. (6) are performed on domain space,
 22 i.e. for completeness sake these equations should have an i,j indicator everywhere designating the
 23 lat/lon location of the gridded domain space. The i,j were not included because it was deemed the
 24 equations would become too complicated unnecessarily. However, the relative error calculated by Eq.
 25 (7), which represents the geometric standard deviation about the expected value as per Martin et al.,
 26 2003, is calculated on the final, total top-down error, ε_t , and *apriori* error, ε_a , which are calculated as
 27 the known summation of error terms, $\varepsilon^2 = \varepsilon_{i,j}^2 + \varepsilon_{i,j+1}^2 + \dots + \varepsilon_{i+1,j}^2 + \varepsilon_{i+1,j+1}^2 + \dots$.



1 In the very recent paper by Cooper et al., 2017, an iterative version of the mass balance methodology
2 [Martin et al., 2003] was shown to provide results of similar accuracy as the more computationally
3 demanding adjoint method [used for e.g. in Stavrakou et al., 2013] in estimating satellite-born NO_x
4 emissions, which encourages the usage of the mass balance technique when one cannot employ from
5 modelling results that calculate an adjoint matrix as well.

6 **3.2 Roadmap of this analysis**

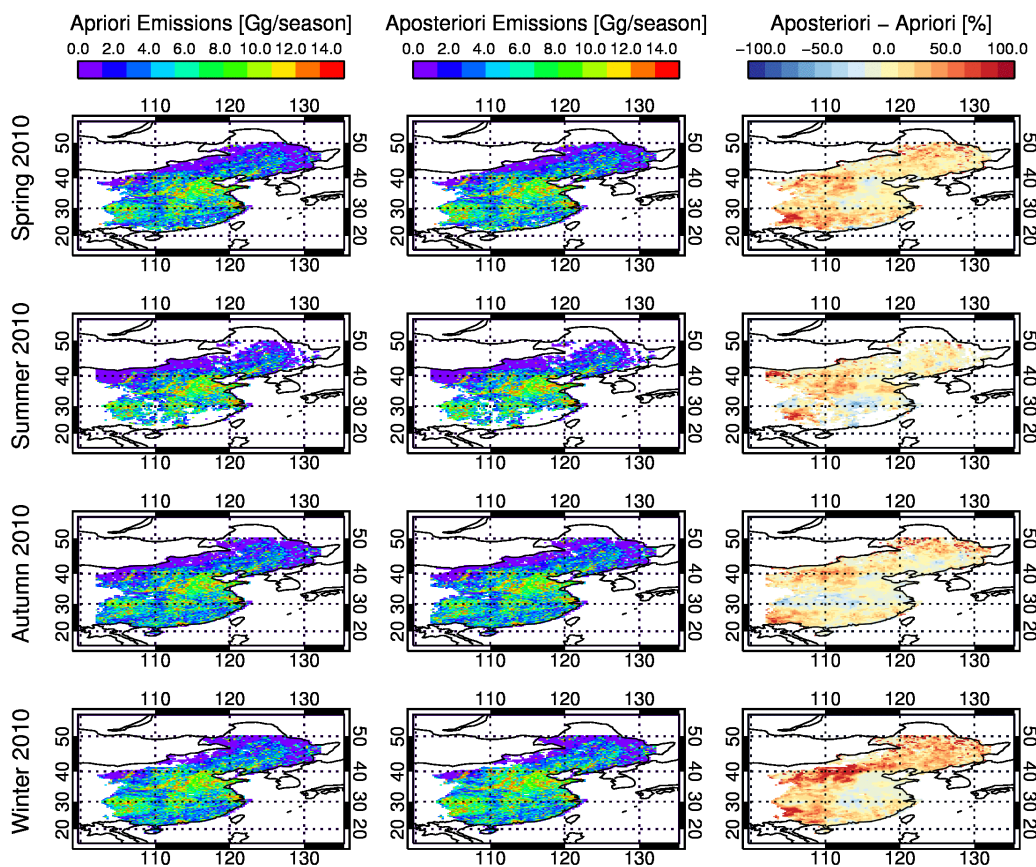
7
8 The statistical methodology described above will be applied to the entire eleven years of OMI/Aura
9 observations, from 2005 to 2015 inclusive. Since the CHIMERE v2013b simulations were performed
10 using the 2010 MEIC v1.2 inventory, year 2010 will be used as reference year in the following analysis.
11 The first step is to present the 2010 updated emissions over the entire domain and how these compare
12 against the *a priori* fields; secondly, monthly mean time series of different locations within the domain
13 are shown and the changes of the SO₂ emissions over the years is discussed. Finally, comparisons
14 against pre-existing bottom-up emission inventories are presented.

15 **4 Results and statistics**

16 **4.1 Updated emissions over China**

17
18 In Figure 5 the seasonal variability of the *a posteriori* emissions calculated with the methodology above
19 are shown in the middle column for spring, summer, autumn and winter [top to bottom.] The
20 equivalent MEIC v1.2 *a priori* inventory on the same seasonal basis is shown in the left column and the
21 percentage differences of the two in the right column. The main take-away message from this pictorial
22 representation of the inventory is that the new inventory is producing higher emissions for the entire
23 domain for all seasons, which are stronger in winter and have positive biases that span from ~10% to
24 ~35% accordingly [Table 1]. Note from the fifth column of the Table the amount of grid points that
25 actually provide information out of an original 8414 grid cells for the domain considered in this work,
26 i.e. the grid cells of the MEIC v1.2 inventory. In the final column of the table, the percentage differences
27 between the two inventories are calculated in two ways: the first value depicts the difference between
28 the first and third columns, i.e. on the sum of emissions for the entire domain. The second value, in
29 square brackets, has been calculated as the mean of the per grid point percentage differences within
30 the domain, hence it contains the geographical deviations of the emission inventories as well. In order
31 to further delve into this geographical variability we present in Figure 6 time series of emissions over
32 four domains of interest; the entire domain studied [18-50°N and 102-132°E], the Greater Beijing region
33 [30-40°N and 110-120°E], the South West region [25-35°N and 100-110°E] and the North East region [40-
34 50°N and 120-130°E]. The two regions in the corners of the area studied were chosen since high SO₂
35 levels were observed by OMI, resulting in increased emissions in the *a posteriori* inventory, that do not
36 appear in the original MEIC v1.2 dataset.

37



1 Figure 5. The seasonal variability of the aposteriori emissions calculated in this work [middle column] in
 2 Gg/season compared to the apriori MEIC v1.2 emissions [left column] in Gg/season as well as their percentage
 3 differences [right column] in %. From top to bottom; spring, summer, autumn and winter of reference year 2010.

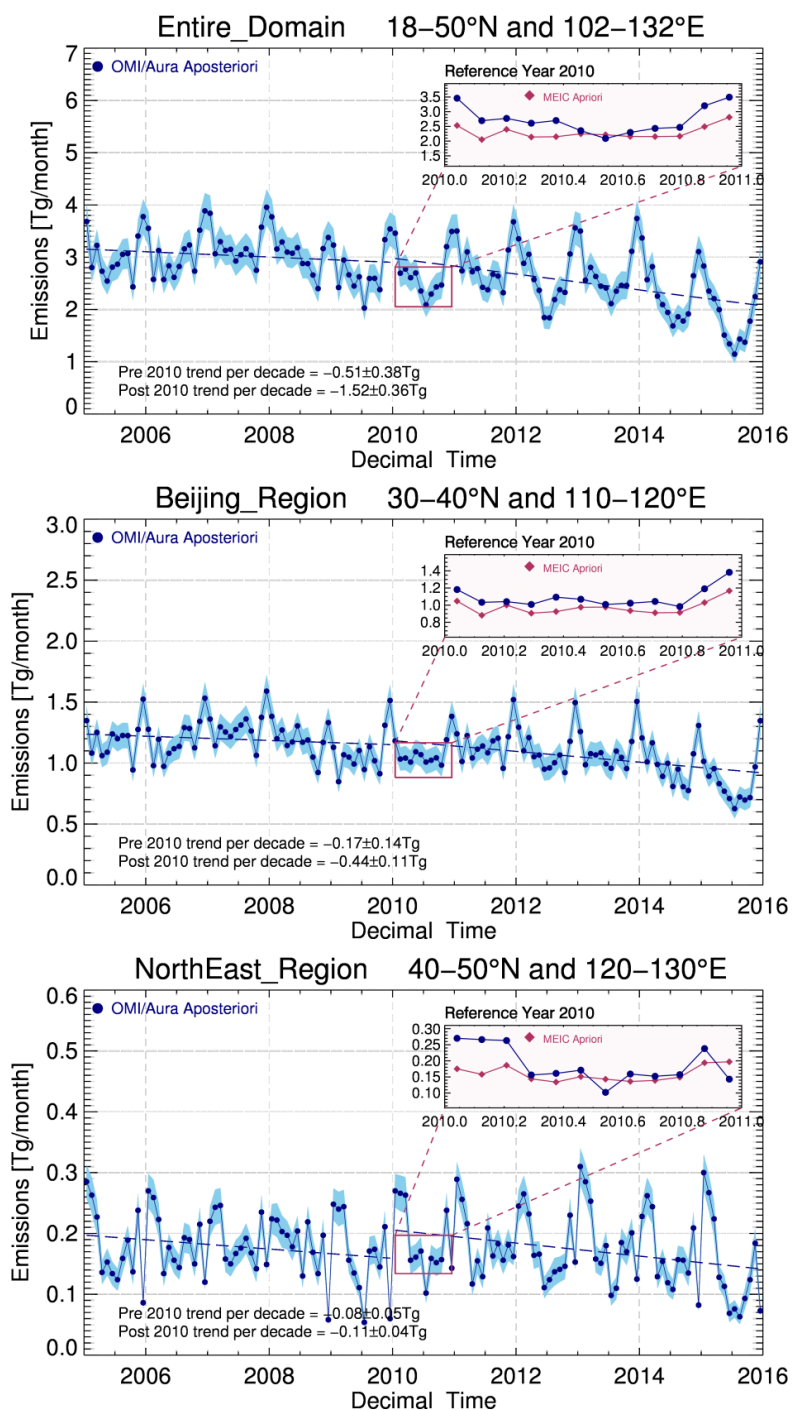
4

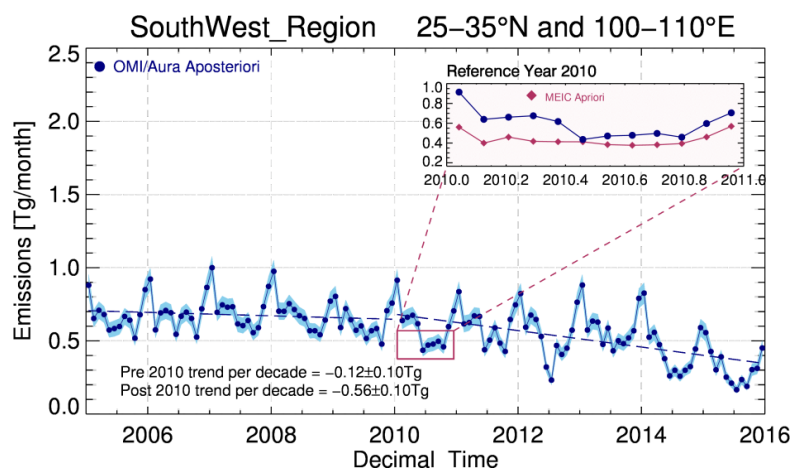
5 Table 1. The average SO₂ emission levels over China for the four seasons of year 2010 as presented in Figure 5.

	Apriori [Gg/season]	Apriori error [Gg/season]	Aposteriori [Gg/season]	Aposteriori error [Gg/season]	# cells	% difference
Spring	6.36	0.135	7.77	1.57	6975	18.0 [24.0]
Summer	5.96	0.132	6.46	1.01	5765	8.0 [14.0]
Autumn	6.77	0.137	7.68	1.40	7126	13.0 [20.0]
Winter	7.07	0.140	9.12	2.66	7254	29.0 [34.0]

6

7





1 Figure 6. Monthly mean time series for the *aposteriori* emissions in Tg/month calculated in this work [dark blue
 2 points] between years 2005 and 2015 inclusive. Insert, the reference year 2010 is shown to include the MEIC v1.2
 3 *apriori* emissions in maroon diamonds. The light blue shaded area depict the calculated *apriori* error [Eq. (7)].
 4 From top to bottom: the entire domain studied [18–50°N and 102–132°E], the Greater Beijing region [30–40°N and
 5 110–120°E], the North East region [40–50°N and 120–130°E] and the South West region [25–35°N and 100–110°E].

6

7 In Figure 6 the monthly mean time series for the *aposteriori* emissions in Tg/month [dark blue lines]
 8 are presented for the four domains of interest, so as to enable a more in depth discussion of the new
 9 inventory. The light blue shaded area depicts the extracted *aposteriori* error on the emissions and the
 10 inset sub-figures depict the reference year 2010 with the *aposteriori* levels shown in blue and the MEIC
 11 v1.2 emissions in maroon. The pre- and post-2010 drifts are also calculated since year 2010 is considered
 12 a turning point as far as regulating SO₂ emissions are concerned [Wang et al., 2015; van der A, et al.,
 13 2016, and references therein]. A very similar picture was shown for all domains: a near-stable decrease
 14 in emissions within the statistical error of the analysis for the pre-2010 levels and a stronger and
 15 statistically significant decrease for the post-2010 levels.

16 For the entire domain [Figure 6, first panel] *aposteriori* emissions on all months show an increase for
 17 year 2010, apart from the JJA summer ones, with the highest increases for the winter months. The pre-
 18 2010 drift is calculated at the limit of the statistical significance, at -0.51 ± 0.38 Tg/month, whereas the
 19 post-2010 drift is stronger and significant at -1.52 ± 0.36 Tg/month. For the greater Beijing region [Figure
 20 6, second panel] a small increase in emissions, nearly constant on all months of 2010, is found with the
 21 post-2010 drift also negative at the -0.44 ± 0.11 Tg/month level. Two special regions of interest, with low
 22 emission levels in general, were revealed by the OMI observations, in the North East and the South
 23 West of the domain and are examined in the third and fourth panels respectively. The first three
 24 months of year 2010 in the *aposteriori* emission database show quite higher levels than the MEIC v1.2
 25 compilation, whereas the rest of the months show the same level, for the NE whereas in the SE the
 26 first six months of the year have an increased SO₂ emitting signature.

27



1 4.2 Comparison with existing emission inventories

2

3 Table 2. Details of the existing emission databases used for comparative purposes.

Database	Years available	Spatial resolution	Temporal resolution	Main reference	Publicly available from:
REASv2.1	2000 to 2008	0.25°x0.25°	monthly	Kurokawa et al., 2013	https://www.nies.go.jp/REAS/
Intex-B	2006	0.5°x0.5°	yearly	Zhang et al., 2009	https://cgrer.uiowa.edu/projects/emmission-data
EDGAR v4.3.1	2010	0.1°x0.1°	monthly	Crippa et al., 2016	http://edgar.jrc.ec.europa.eu/

4

5 Apart from the MEIC v1.2 emission inventory discussed in Section 2.1, which is currently publicly
6 available for years 2008, 2010 and 2012, there exist other emission inventories that are frequently used
7 in chemical transport models as input; the Regional Emission inventory in Asia (REAS) v2.1 [Kurokawa
8 et al., 2013]; the 2006 Asia Emissions for Intex-B [Zhang et al., 2009] and the Emissions Database for
9 Global Atmospheric Research, EDGAR v4.3.1 [Crippa et al., 2016]. Comparing with similar published
10 works is not as straightforward as one would assume since in this work a sub-domain of what is termed
11 *China* in other publications is used. For e.g. when calculating the total annual SO₂ emissions reported
12 by the REASv2.1 database for year 2000, those are found to be 25.62Tg per annum when allowing the
13 entire domain provided in the database but only rise to 15.86Tg per annum when restricting in the
14 domain we are studying. As a result, large differences and erroneous comparisons may be presented
15 if one simply compares emissions estimates as reported in published works. For completion purposes
16 we refer the reader to Table 3 of Lu et al., 2010 and Table 8 of Kurokawa et al., 2013, for similar
17 comparative studies, however great care is needed when quoting absolute SO₂ emission levels.

18 In Table 2 the details of the three databases are given. Since we are interested in evaluating SO₂
19 emission fields and not point source levels, we focused on these three databases which provide their
20 databases in actual spatiotemporal resolutions. As a first inspection, in Table 3, the annual SO₂
21 emissions for the domain 102°E - 132°E and 15°N - 50°N in Tg per annum are presented. We should point
22 out that, due to the fact that our methodology is based on the MEIC v1.2 emission inventory, within
23 the domain stated there are large areas with no emissions, mostly over sea and the Korean peninsula.
24 In the following comparisons, only the common pixels between all inventories are used for the
25 calculations naturally.

26 Several issues arise; firstly, for the common years between this work and the REAS v2.1, i.e. years 2005
27 to 2008 inclusive, the differences span between ~30 and ~60% with REAS v2.1 underestimating the
28 emission levels in the domain studied. For the one common year between REAS v2.1 and MEIC v1.2,
29 namely 2008, this underestimation still holds but is smaller, of the order of ~10%. Similarly, for the one
30 common year between REAS v2.1 and Intex-B, namely 2006, REAS v2.1 underestimates by ~30%. All
31 these point to an underestimation of SO₂ levels in the domain considered by the REAS v2.1 database.

32 Comparing the 2006 Intex-B emissions to the ones calculated in this work, we find a difference of the
33 order of ~10% whereas comparing to the 2010 EDGAR v4.3.1 emissions the difference is almost



1 insignificant, at ~3.5%. Since the EDGAR v4.3.1 emissions are provided on a monthly basis, in contrast
 2 to the Intex-B ones, we can evaluate our spatial patterns as well. After regridding the EDGAR v4.3.1
 3 emissions onto a 0.25°x0.25° spatial resolution on a monthly basis, the seasonal variability of the
 4 inventory is compared to the one presented in this work in Figure 7.

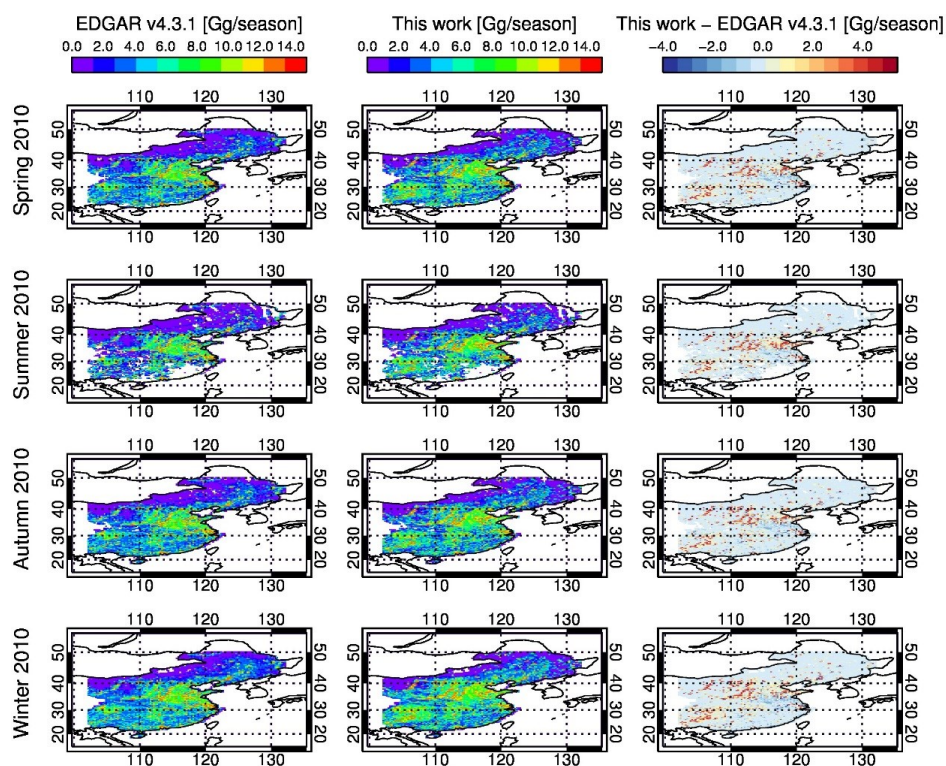
5

6 Table 3. Annual SO₂ emissions over the domain 102°E - 132°E and 15°N - 50°N in Tg per annum; first column the
 7 year; second column this work; third column the REASv2.1; fourth column, EDGAR v4.3.1 and fifth column, the
 8 Intex-B database.

Year	This work	REASv2.1	MEIC v1.2	EDGAR v4.3.1	Intex-B
	Tg/annum for the 102°E - 132°E and 15°N - 50°N domain				
2000		15.86			
2001		15.94			
2002		17.53			
2003		19.70			
2004		21.77			
2005	35.27±1.75	24.68			
2006	35.33±1.76	24.45			32.08
2007	37.58±1.76	24.40			
2008	35.75±1.76	26.96	29.80		
2009	31.74±1.75				
2010	32.14±1.74		26.26	33.34	
2011	33.50±1.75				
2012	31.30±1.75		26.48		
2013	32.05±1.74				
2014	28.32±1.72				
2015	23.34±1.71				

9

10



1 Figure 7. The seasonal variability of the a posteriori emissions calculated in this work [middle column] in
 2 Gg/season compared to the EDGAR v4.3.1 emissions [left column] in Gg/season as well as their absolute
 3 differences [right column]. From top to bottom; spring, summer, autumn and winter of the reference year 2010.

4

5 Summary

6

7 In this work, an updated SO₂ emission inventory based on OMI/Aura observations and the CHIMERE
 8 v2013b simulations has been presented for years 2005 to 2015 inclusive, as part of the EU FP7
 9 MarcoPolo project which provides updated emissions over China based on satellite observations of
 10 key air quality species. For the domain between 102°E - 132°E and 15°N - 50°N it was shown that the
 11 annual SO₂ emissions calculated remain stable at 36.0±1.0 Tg/annum between years 2005 and 2008,
 12 decreasing to 32±0.8Tg/annum between 2008 and 2010, leading to a low of ~23.0 Tg/annum for year
 13 2015, with highs during the winter months and lows during the spring and summer time. Trend analysis
 14 performed on the monthly mean spatial averages show that pre-2010, the monthly SO₂ emissions were
 15 ~3.0±1.0 Tg/month whereas the statistically significant decrease in the post-2010 era rises to -1.52±0.36
 16 Tg. The higher differences to the original a priori MEIC v1.2 2010 inventory were found for the winter
 17 months, especially February, with seasonal differences of the order of ~40% and the smallest for the
 18 summer months at ~10%. Comparisons with completely independent emission inventories show a good



1 agreement to the 2010 EDGAR v4.3.1 emissions at the 3.5% level, whereas moderate agreement was
2 found against the 2006 Intex-B database at the ~10% level.

3 The subsequent logical step in this work is to employ the new emission inventory as input information
4 for a chemistry transport model so as to assess the effect of the updated SO₂ emissions on the output
5 simulations, as well as validation against independent sources of information on the point SO₂ sources
6 around China, a work under development.

7 **Data availability**

8

9 Input datasets:

10 OMI/Aura SO₂ BIRA algorithm, main reference: Theys, N., De Smedt, I., van Gent, J., et al., (2015), Sulfur
11 dioxide vertical column DOAS retrievals from the Ozone Monitoring Instrument: Global
12 observations and comparison to ground-based and satellite data, *J. Geophys. Res. Atmos.*, 120(6),
13 2470–2491, doi:10.1002/2014JD022657.

14 CHIMERE v2013b simulations, main reference: Ding, J., van der A, R. J., Mijling, B., Levelt, P. F., and Hao,
15 N.: NO_x emission estimates during the 2014 Youth Olympic Games in Nanjing, *Atmos. Chem. Phys.*,
16 15, 9399–9412, doi:10.5194/acp-15-9399-2015, 2015.

17 Output datasets:

18 EU FP7 MarcoPolo SO₂ emission inventory is publicly available from [http://www.marcopolo-
panda.eu/products/toolbox/emission-data/](http://www.marcopolo-
19 panda.eu/products/toolbox/emission-data/) and the main reference is this work.

20 Auxiliary datasets:

21 The MEIC v1.2 database is publicly available from <http://www.meicmodel.org/> and the main reference
22 is n/a.

23 The Intex-B database is publicly available from <https://cgrer.uiowa.edu/projects/emmission-data> and the
24 main reference is Zhang, Q., D.G. Streets, G.R. Carmichael, et al., (2009), Asian emissions in 2006
25 for the NASA INTEX-B mission, *Atmos. Chem. Phys.*, 9, 5131–5153, doi:10.5194/acp-9-5131-2009.

26 The EDGAR v4.3.1 database is publicly available from <http://edgar.jrc.ec.europa.eu/> and the main
27 reference is Crippa, M., Janssens-Maenhout, G., Dentener, F., Guizzardi, D., Sindelarova, K.,
28 Muntean, M., Van Dingenen, R., and Granier, C.: Forty years of improvements in European air
29 quality: regional policy-industry interactions with global impacts, *Atmos. Chem. Phys.*, 16, 3825-
30 3841, doi:10.5194/acp-16-3825-2016, 2016.

31 The REAS v2.1 database is publicly available from <https://www.nies.go.jp/REAS/> and the main reference
32 is Kurokawa, J., Ohara, T., Morikawa, T., Hanayama, S., Janssens-Maenhout, G., Fukui, T.,
33 Kawashima, K., and Akimoto, H.: Emissions of air pollutants and greenhouse gases over Asian
34 regions during 2000–2008: Regional Emission inventory in ASia (REAS) version 2, *Atmos. Chem.*
35 *Phys.*, 13, 11019–11058, doi:10.5194/acp-13-11019-2013, 2013.

36
37



1

2 **Acknowledgements**

3

4 This work has been funded by the EU FP7 MarcoPolo project, www.marcopolo.eu, 2014-2017. Results
5 presented in this work have been produced using the European Grid Infrastructure (EGI) through the
6 National Grid Infrastructures NGI_GRNET (HellasGrid) as part of the SEE Virtual Organization. The
7 authors would like to acknowledge the support provided by the Scientific Computing Office, IT A.U.Th.,
8 throughout the progress of this research work. We wholeheartedly thank Ass. Prof. Eleni Katragkou
9 for her assistance with the ERA Interim datasets.

10

11 **References**

12

- 13 Bauduin, S., Clarisse, L., Hadji-Lazaro, J., Theys, N., Clerbaux, C., and Coheur, P.-F.: Retrieval of near-
14 surface sulfur dioxide (SO₂) concentrations at a global scale using IASI satellite observations,
15 Atmos. Meas. Tech., 9, 721-740, doi:10.5194/amt-9-721-2016, 2016.
- 16 Boersma, K. F., D. J. Jacob, H. J. Eskes, R. W. Pinder, J. Wang, and R. J. van der A (2008a),
17 Intercomparison of SCIAMACHY and OMI tropospheric NO₂ columns: Observing the diurnal
18 evolution of chemistry and emissions from space, J. Geophys. Res., 113, D16S26,
19 doi:10.1029/2007JD008816.
- 20 Boersma, K. F., D.J. Jacob, E.J. Bucsela, A.E. Perring, R. Dirksen, R.J. van der A, R.M. Yantosca, R.J. Park,
21 M.O. Wenig, T.H. Bertram, R.C. Cohen, Validation of OMI tropospheric NO observations during
22 INTEX-B and application to constrain emissions over the eastern United States and Mexico,
23 Atmospheric Environment, <http://dx.doi.org/10.1016/j.atmosenv.2008.02.004>, 2008b.
- 24 Boersma, K. F., Vinken, G. C. M., and Eskes, H. J. (2016), Representativeness errors in comparing
25 chemistry transport and chemistry climate models with satellite UV-Vis tropospheric column
26 retrievals, Geosci. Model Dev., 9, 875-898, doi:10.5194/gmd-9-875-2016.
- 27 Ceccherini, S. and Ridolfi, M.: Technical Note: Variance-covariance matrix and averaging kernels for the
28 Levenberg-Marquardt solution of the retrieval of atmospheric vertical profiles, Atmos. Chem.
29 Phys., 10, 3131-3139, doi:10.5194/acp-10-3131-2010, 2010.
- 30 Cooper, M., R. V. Martin, A. Padmanabhan, and D. K. Henze (2017), Comparing mass balance and
31 adjoint methods for inverse modeling of nitrogen dioxide columns for global nitrogen oxide
32 emissions, J. Geophys. Res. Atmos., 122, 4718-4734, doi:10.1002/2016JD025985.
- 33 Crippa, M., Janssens-Maenhout, G., Dentener, F., Guizzardi, D., Sindelarova, K., Muntean, M.,
34 Van Dingenen, R., and Granier, C.: Forty years of improvements in European air quality: regional
35 policy-industry interactions with global impacts, Atmos. Chem. Phys., 16, 3825-3841,
36 doi:10.5194/acp-16-3825-2016, 2016.



- 1 De Smedt, I., Van Roozendaal, M., Stavrou, T., Müller, J.-F., Lerot, C., Theys, N., Valks, P., Hao, N., and
2 van der A, R., (2012), Improved retrieval of global tropospheric formaldehyde columns from
3 GOME-2/MetOp-A addressing noise reduction and instrumental degradation issues, *Atmos. Meas.*
4 *Tech.*, 5, 2933-2949, doi:10.5194/amt-5-2933-2012.
- 5 Dee, D. P., Uppala, S. M., Simmons, A. J., Berrisford, P., Poli, P., Kobayashi, S., Andrae, U., Balmaseda,
6 M. A., Balsamo, G., Bauer, P., Bechtold, P., Beljaars, A. C. M., van de Berg, L., Bidlot, J., Bormann,
7 N., Delsol, C., Dragani, R., Fuentes, M., Geer, A. J., Haimberger, L., Healy, S. B., Hersbach, H., Hólm,
8 E. V., Isaksen, I., Kållberg, P., Köhler, M., Matricardi, M., McNally, A. P., Monge-Sanz, B. M.,
9 Morcrette, J.-J., Park, B.-K., Peubey, C., de Rosnay, P., Tavolato, C., Thépaut, J.-N. and Vitart, F.
10 (2011), The ERA-Interim reanalysis: configuration and performance of the data assimilation system.
11 *Q.J.R. Meteorol. Soc.*, 137: 553–597. doi:10.1002/qj.828
- 12 Deguillaume, L., M. Beekmann, and C. Derognat (2008), Uncertainty evaluation of ozone production
13 and its sensitivity to emission changes over the Ile-de-France region during summer periods, *J.*
14 *Geophys. Res.*, 113, D02304, doi:10.1029/2007JD009081.
- 15 Ding, J., van der A, R. J., Mijling, B., Levelt, P. F., and Hao, N.: NO_x emission estimates during the 2014
16 Youth Olympic Games in Nanjing, *Atmos. Chem. Phys.*, 15, 9399-9412, doi:10.5194/acp-15-9399-2015,
17 2015.
- 18 Eskes, H. J. and Boersma, K. F.: Averaging kernels for DOAS total-column satellite retrievals, *Atmos.*
19 *Chem. Phys.*, 3, 1285-1291, doi:10.5194/acp-3-1285-2003, 2003.
- 20 Fioletov, V. E., C. A. McLinden, N. Krotkov, and C. Li (2015), Lifetimes and emissions of SO₂ from point
21 sources estimated from OMI. *Geophys. Res. Lett.*, 42, 1969–1976. doi: 10.1002/2015GL063148.
- 22 Fioletov, V. E., et al. (2013), Application of OMI, SCIAMACHY, and GOME-2 satellite SO₂ retrievals for
23 detection of large emission sources, *J. Geophys. Res. Atmos.*, 118, 11,399–11,418,
24 doi:10.1002/jgrd.50826.
- 25 Fioletov, V. E., McLinden, C. A., Krotkov, N., Li, C., Joiner, J., Theys, N., Carn, S., and Moran, M. D.: A
26 global catalogue of large SO₂ sources and emissions derived from the Ozone Monitoring
27 Instrument, *Atmos. Chem. Phys.*, 16, 11497-11519, doi:10.5194/acp-16-11497-2016, 2016.
- 28 Gu, D., Y. Wang, C. and K. F. Boersma, (2014), Anthropogenic emissions of NO_x over China: Reconciling
29 the difference of inverse modeling results using GOME-2 and OMI measurements, *Journal of*
30 *Geophysical Research: Atmospheres*, <http://dx.doi.org/10.1002/2014JD021644>.
- 31 Hains, J. C., B. F. Taburn, A. M. Thompson, J. W. Stehr, L. T. Marufu, B. G. Doddridge, and R. R.
32 Dickerson (2008), Origins of chemical pollution derived from mid-Atlantic aircraft profiles using a
33 clustering technique, *Atmos. Environ.*, 42, 1727–1741, doi:10.1016/j.atmosenv.2007.11.052.
- 34 Jiang, J., Zha, Y., Gao, J., and Jiang, J. (2012), Monitoring of SO₂ column concentration change over
35 China from Aura OMI data, *Int. J. Remote Sens.*, 33, 1934–1942, doi:10.1080/01431161.2011.603380.
- 36 Kan, Haidong, Renjie Chen and Shilu Tong, (2012), Ambient air pollution, climate change, and
37 population health in China, *Environment International*, <https://doi.org/10.1016/j.envint.2011.03.003>.
- 38 Klimont, Z., Smith, S. J. and Cofala, J., (2013), The last decade of global anthropogenic sulfur dioxide:
39 2000–2011 emissions, *Environ. Res. Lett.*, 8(1), 014003, doi:10.1088/1748-9326/8/1/014003.



- 1 Koukoulis, M. E., D.S. Balis, R. van der A, N. Theys, P. Hedelt, A. Richter, N. Krotkov, C. Li, M. Taylor,
2 (2016), Anthropogenic sulphur dioxide load over China as observed from different satellite
3 sensors, *Atmospheric Environment*, <http://dx.doi.org/10.1016/j.atmosenv.2016.09.007>.
- 4 Krotkov, N. A., et al. (2008), Validation of SO₂ retrievals from the Ozone Monitoring Instrument over
5 NE China, *J. Geophys. Res.*, 113, D16S40, doi:[10.1029/2007JD008818](https://doi.org/10.1029/2007JD008818).
- 6 Kurokawa, J., Ohara, T., Morikawa, T., Hanayama, S., Janssens-Maenhout, G., Fukui, T., Kawashima, K.,
7 and Akimoto, H.: Emissions of air pollutants and greenhouse gases over Asian regions during
8 2000–2008: Regional Emission inventory in ASia (REAS) version 2, *Atmos. Chem. Phys.*, 13, 11019–
9 11058, doi:10.5194/acp-13-11019-2013, 2013.
- 10 Lamsal, L. N., R. V. Martin, A. van Donkelaar, E. A. Celarier, E. J. Bucsela, K. F. Boersma, R. Dirksen, C.
11 Luo, and Y. Wang (2010), Indirect validation of tropospheric nitrogen dioxide retrieved from the
12 OMI satellite instrument: Insight into the seasonal variation of nitrogen oxides at northern
13 midlatitudes, *J. Geophys. Res.*, doi:10.1029/2009JD013351.
- 14 Lee, C., R. V. Martin, A. van Donkelaar, G. O'Byrne, N. Krotkov, A. Richter, L. G. Huey, and J. S. Holloway
15 (2009), Retrieval of vertical columns of sulfur dioxide from SCIAMACHY and OMI: Air mass factor
16 algorithm development, validation, and error analysis, *J. Geophys. Res.*, 114, D22303,
17 doi:10.1029/2009JD012123.
- 18 Lee, C., R. V. Martin, A. van Donkelaar, H. Lee, R. R. Dickerson, J. C. Hains, N. Krotkov, A. Richter, K.
19 Vinnikov, and J. J. Schwab (2011), SO₂ emissions and lifetimes: Estimates from inverse modeling
20 using in situ and global, space-based (SCIAMACHY and OMI) observations, *J. Geophys. Res.*, 116,
21 D06304, doi:[10.1029/2010JD014758](https://doi.org/10.1029/2010JD014758).
- 22 Leue, C., M. Wenig, T. Wagner, et al. (2001), Quantitative analysis of NO_x emissions from Global Ozone
23 Monitoring Experiment satellite image sequences, *J. Geophys. Res.*, 106(D6), 5493–5505,
24 doi:10.1029/2000JD900572.
- 25 Li, C., Zhang, Q., Krotkov, N. A., Streets, D. G., He, K., Tsay, S.-C., and Gleason, J. F. (2010), Recent large
26 reduction in sulphur dioxide emissions from Chinese power plants observed by the Ozone
27 Monitoring Instrument, *Geophys. Res. Lett.*, 37, L08807, doi:10.1029/2010GL042594.
- 28 Lin, J.-T., McElroy, M. B., and Boersma, K. F. (2010), Constraint of anthropogenic NO_x emissions in
29 China from different sectors: a new methodology using multiple satellite retrievals, *Atmos. Chem.*
30 *Phys.*, 10, 63–78, doi:10.5194/acp-10-63-2010.
- 31 Liu, F., Zhang, Q., Tong, D., Zheng, B., Li, M., Huo, H., and He, K. B., (2015), High-resolution inventory of
32 technologies, activities, and emissions of coal-fired power plants in China from 1990 to 2010,
33 *Atmos. Chem. Phys.*, doi:10.5194/acp-15-13299-2015.
- 34 Liu, Fei, Qiang Zhang, Ronald J van der A, Bo Zheng, Dan Tong, Liu Yan, Yixuan Zheng and Kebin He
35 (2017), Recent reduction in NO_x emissions over China: synthesis of satellite observations and
36 emission inventories, *Environmental Research Letters*, [http://dx.doi.org/10.1088/1748-](http://dx.doi.org/10.1088/1748-9326/11/11/114002)
37 [9326/11/11/114002](http://dx.doi.org/10.1088/1748-9326/11/11/114002).



- 1 Lu Feng and Wenjie Liao, (2016), Legislation, plans, and policies for prevention and control of air
2 pollution in China: achievements, challenges, and improvements, *Journal of Cleaner Production*,
3 <https://doi.org/10.1016/j.jclepro.2015.08.013>.
- 4 Lu, Z., Streets, D. G., Zhang, Q., et al., (2010), Sulfur dioxide emissions in China and sulfur trends in East
5 Asia since 2000, *Atmos. Chem. Phys.*, doi:10.5194/acp-10-6311-2010.
- 6 Lu, Z., Zhang, Q., and Streets, D. G., (2011) Sulfur dioxide and primary carbonaceous aerosol emissions
7 in China and India, 1996–2010, *Atmos. Chem. Phys.*, doi:10.5194/acp-11-9839-2011.
- 8 Martin, R. V., C. E. Sioris, K. Chance, et al. (2006), Evaluation of space-based constraints on global
9 nitrogen oxide emissions with regional aircraft measurements over and downwind of eastern
10 North America, *J. Geophys. Res.*, 111, D15308, doi:10.1029/2005JD006680.
- 11 Martin, R. V., D. J. Jacob, K. Chance, et al. (2003), Global inventory of nitrogen oxide emissions
12 constrained by space-based observations of NO₂ columns, *J. Geophys. Res.*, 108, 4537,
13 doi:10.1029/2003JD003453, D17.
- 14 Menut, L., Bessagnet, B., Khvorostyanov, D., Beekmann, M., Blond, N., Colette, A., Coll, I., Curci, G.,
15 Foret, G., Hodzic, A., Mailler, S., Meleux, F., Monge, J.-L., Pison, I., Siour, G., Turquety, S., Valari, M.,
16 Vautard, R., and Vivanco, M. G., (2013), CHIMERE 2013: a model for regional atmospheric
17 composition modelling, *Geosci. Model Dev.*, 6, 981-1028, doi:10.5194/gmd-6-981-2013.
- 18 Mijling, B., and R. J. van der A (2012), Using daily satellite observations to estimate emissions of short-
19 lived air pollutants on a mesoscopic scale, *J. Geophys. Res.*, 117, D17302, doi:10.1029/2012JD017817
- 20 Pirovano, G., et al., (2012), Investigating impacts of chemistry and transport model formulation on
21 model performance at European scale, *Atmospheric Environment*,
22 doi:10.1016/j.atmosenv.2011.12.052
- 23 Rodgers, C. D.: *Inverse Methods for Atmospheric Sounding: Theory and Practice*, World Sci.,
24 Hackensack, N. J., 2000.
- 25 Schmidt, A., S. Leadbetter, N. Theys, E. Carboni, C. S. Witham, J. A. Stevenson, C. E. Birch, T. Thordarson,
26 S. Turnock, S. Barsotti, et al., Satellite detection, long-range transport, and air quality impacts of
27 volcanic sulfur dioxide from the 2014–2015 flood lava eruption at Bárðarbunga (Iceland), *J.*
28 *Geophys. Res. Atmos.*, 120, 9739–9757, doi:10.1002/2015JD023638, 2015.
- 29 Seinfeld, J. H. and S. N. Pandis, *Atmospheric Chemistry and Physics: From Air Pollution to Climate*
30 *Change*, John Wiley and Sons, 1998
- 31 Smith, S. J., Hugh Pitcher and T.M.L Wigley, (2001), Global and regional anthropogenic sulfur dioxide
32 emissions, *Global and Planetary Change*, [https://doi.org/10.1016/S0921-8181\(00\)00057-6](https://doi.org/10.1016/S0921-8181(00)00057-6).
- 33 Smith, S. J., van Aardenne, J., Klimont, Z., Andres, R. J., Volke, A., and Delgado Arias, S., (2011),
34 Anthropogenic sulfur dioxide emissions: 1850–2005, *Atmos. Chem. Phys.*, 11, 1101-1116,
35 doi:10.5194/acp-11-1101-2011.
- 36 Song, Congbo, Lin Wu, Yaochen Xie, Jianjun He, Xi Chen, Ting Wang, Yingchao Lin, Taosheng Jin, Anxu
37 Wang, Yan Liu, Qili Dai, Baoshuang Liu, Ya-nan Wang, Hongjun Mao, (2017), Air pollution in China:



- 1 Status and spatiotemporal variations, Environmental Pollution,
2 <https://doi.org/10.1016/j.envpol.2017.04.075>.
- 3 Stavrakou, T., J.-F. Müller, K. F. Boersma, R. J. van der A, J. Kurokawa, T. Ohara, and Q. Zhang (2013),
4 Key chemical NO_x sink uncertainties and how they influence top-down emissions of nitrogen
5 oxides, Atmos. Chem. Phys., 13, 9057–9082, doi:10.5194/acp-13-9057-2013.
- 6 Streets, David G., Timothy Canty, Gregory R. Carmichael, Benjamin de Foy, Russell R. Dickerson, Bryan
7 N. Duncan, David P. Edwards, John A. Haynes, Daven K. Henze, Marc R. Houyoux, Daniel J. Jacob,
8 Nickolay A. Krotkov, Lok N. Lamsal, Yang Liu, Zifeng Lu, Randall V. Martin, Gabriele G. Pfister,
9 Robert W. Pinder, Ross J. Salawitch, Kevin J. Wecht (2013), Emissions estimation from satellite
10 retrievals: A review of current capability, Atmospheric Environment,
11 <https://doi.org/10.1016/j.atmosenv.2013.05.051>.
- 12 Theys, N., De Smedt, I., van Gent, J., et al., (2015), Sulfur dioxide vertical column DOAS retrievals from
13 the Ozone Monitoring Instrument: Global observations and comparison to ground-based and
14 satellite data, J. Geophys. Res. Atmos., 120(6), 2470–2491, doi:10.1002/2014JD022657.
- 15 Theys, N., De Smedt, I., Yu, H., Danckaert, T., van Gent, J., Hörmann, C., Wagner, T., Hedelt, P., Bauer,
16 H., Romahn, F., Pedernana, M., Loyola, D., and Van Roozendael, M.: Sulfur dioxide retrievals from
17 TROPOMI onboard Sentinel-5 Precursor: algorithm theoretical basis, Atmos. Meas. Tech., 10, 119-
18 153, doi:10.5194/amt-10-119-2017, 2017.
- 19 van der A, R. J., Mijling, B., Ding, J., Koukouli, M. E., Liu, F., Li, Q., Mao, H., and Theys, N., (2016), Cleaning
20 up the air: Effectiveness of air quality policy for SO₂ and NO_x emissions in China, Atmos. Chem.
21 Phys. Discuss., doi:10.5194/acp-2016-445.
- 22 Wang, Siwen, David G Streets, Qiang Zhang, Kebin He, Dan Chen, Sicong Kang, Zifeng Lu and Yuxuan
23 Wang, (2010), Satellite detection and model verification of NO_x emissions from power plants in
24 Northern China, Environmental Research Letters, <http://dx.doi.org/10.1088/1748-9326/5/4/044007>
- 25 Wang, Siwen, Qiang Zhang, Randall V Martin, Sajeev Philip, Fei Liu, Meng Li, Xujia Jiang and Kebin He
26 (2015), Satellite measurements oversee China's sulfur dioxide emission reductions from coal-fired
27 power plants, Environmental Research Letters, <http://dx.doi.org/10.1088/1748-9326/10/11/114015>.
- 28 Wang, Y., Beirle, S., Lampel, J., Koukouli, M., De Smedt, I., Theys, N., Li, A., Wu, D., Xie, P., Liu, C., Van
29 Roozendael, M., Stavrakou, T., Müller, J.-F., and Wagner, T.: Validation of OMI, GOME-2A and
30 GOME-2B tropospheric NO₂, SO₂ and HCHO products using MAX-DOAS observations from 2011 to
31 2014 in Wuxi, China: investigation of the effects of priori profiles and aerosols on the satellite
32 products, Atmos. Chem. Phys., 17, 5007-5033, doi:10.5194/acp-17-5007-2017, 2017.
- 33 Witte, J. C., Schoeberl, M. R., Douglass, A. R., Gleason, J. F., Krotkov, N. A., Gille, J. C., Pickering, K. E.,
34 and Livesey, N. (2009), Satellite observations of changes in air quality during the 2008 Beijing
35 Olympics and Paralympics, Geophys. Res. Lett., 36, L17803, doi:10.1029/2009GL039236.
- 36 Zhang, L., Jacob, D. J., Liu, X., Logan, J. A., Chance, K., Eldering, A., and Bojkov, B. R.: Intercomparison
37 methods for satellite measurements of atmospheric composition: application to tropospheric
38 ozone from TES and OMI, Atmos. Chem. Phys., 10, 4725-4739, doi:10.5194/acp-10-4725-2010, 2010.



- 1 Zhang, Q. Q., Wang, Y., Ma, Q., Yao, Y., Xie, Y., and He, K., (2015) Regional differences in Chinese SO₂
2 emission control efficiency and policy implications, *Atmos. Chem. Phys.*, 15, 6521-6533,
3 doi:10.5194/acp-15-6521-2015.
- 4 Zhang, Q., D.G. Streets, G.R. Carmichael, et al., (2009), Asian emissions in 2006 for the NASA INTEX-B
5 mission, *Atmos. Chem. Phys.*, 9, 5131-5153, doi:10.5194/acp-9-5131-2009.
- 6 Zhang, Q., K. He, H. Huo, (2012), Cleaning China's air, *Nature*, 484, 161–162, doi:/10.1038/484161a.
- 7 Zhou, Y., Brunner, D., Boersma, K. F., Dirksen, R., and Wang, P., An improved tropospheric NO₂
8 retrieval for OMI observations in the vicinity of mountainous terrain, *Atmos. Meas. Tech.*,
9 doi:10.5194/amt-2-401-2009, 2009.
- 10 Zyrichidou, I., M.E. Koukouli, D. Balis, K. Markakis, A. Poupkou, E. Katragkou, I. Kioutsoukis, D. Melas,
11 K.F. Boersma, M. van Roozendaal, Identification of surface NO emission sources on a regional
12 scale using OMI NO, *Atmospheric Environment*, <http://dx.doi.org/10.1016/j.atmosenv.2014.11.023>,
13 2015.